Satellite Formation Flying for High-Precision Earth Observation

Pol Francesch Huc, Sydney Hsu

AA 279D - Spacecraft Formation-Flying and Rendezvous
Stanford University

Revision History

Table 1: Summary of project revisions.

Rev	Changes
PS1	- Created document - Added problem set 1 material

Contents

List of Figures

List of Tables

1 Scope

This report introduces the project, mission specifications, and absolute orbit simulation for AA279D Dynamics, Navigation and Control of Distributed Space Systems.

2 Problem Set 1

2.1 Problem 1: Your Mission, Your Challenge

Reference Mission

This project is based on TanDEM-X, a formation-flying satellite mission performing Earth observation using interferometric Synthetic Aperture Radar (SAR) measurements to create a Digital Elevation Model (DEM). TanDEM-X was launched as an extension to join its twin TerraSAR-X and both satellites are operated by the German Aerospace Center (DLR). Data is managed and distributed by the European Space Agency (ESA), and the satellites were built by Airbus Defense and Space [1].

Mission Objectives

The primary goal of the mission is to create high-precision 3-dimensional models of the Earth's surface to the High-Resolution Terrain Elevation Level 3 (HRTE-3) model specification as defined by the National Geospatial Agency. Images produced by the SAR instruments aids monitoring of land and coastal processes such as vegetation, glacial melt, and ocean currents. Moreover, pole-to-pole global data provided by this mission is critical across a range of science, government, military, and commercial applications. The secondary objective of TanDEM-X is to demonstrate novel SAR techniques (including digital beamforming, along-track interferometry with a varying baseline, and super-resolution). Additionally, this mission demonstrates a new orbit concept allowing for safe formation flying at close proximity between the two spacecraft [1].

Before TanDEM-X, previous DEMs lacked full global coverage and precision required for modern navigation, military operations, and scientific applications [2]. As shown in Table 2, the novel DEM standard generated by TanDEM-X (HRTI-3) compared to the previous state-of-the-art (DTED-2) is significantly more accurate across the board, and provides spatial resolution that is sharper by more than a factor of 2.

Table 2: Comparison of DTED-2 and HRTE-3 specifications [2]

Requirement	Specification	DTED-2	HRTI-3
Relative Vertical Accuracy	90% linear point-to-point error over a 1° x 1° cell	12 m (slope < 20%) 15 m (slope > 20%)	2 m (slope < 20%) 4 m (slope > 20%)
Absolute Vertical Accuracy	90% linear error	18 m	10 m
Relative Horizontal Accuracy	90% circular error	15 m	3 m
Horizontal Accuracy	90% circular error	23 m	10 m
Spatial Resolution	independent pixels	30 m (1 arc sec @ equator)	12 m (0.4 arc sec @ equator)

Spacecraft Specification

The mission relies on formation flying involving the TanDEM-X and TerraSAR-X satellites. The two satellites were built nearly identical and are equipped with identical X-band SAR instruments to collect high-resolution Earth images. The main difference between the two satellites is that TanDEM-X features an inter-satellite S-band receiver which it uses to receive status and GPS information from TerraSAR-X. It also has been upgraded with an advanced cold-gas propulsion system for fine formation-keeping maneuvers [1] [2].

TerraSAR-X has a wet mass of 1230 kg (of which 78 kg are propellant) and have dimensions of 5m x 2.4 m. While TanDEM-X has the same dimensions, it is heavier at 1340 wet mass (of which 120 kg are propellant). The SAR antennas have dimensions of 5 m x 0.8 m. The average orbit power and end-of-life is 800 W [1] [3].

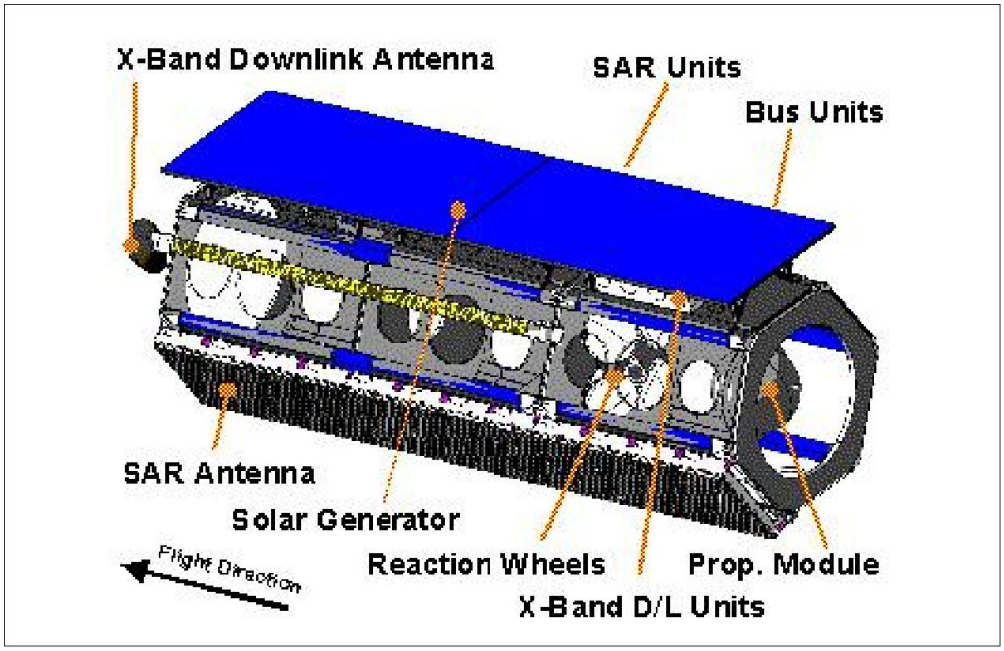

Figure 1: TerraSAR-X spacecraft features. [3]

Launch and Orbit

TerraSAR-X remains in the sun-synchronous dawn-dusk orbit at which it was launched. Its orbit is described by a mean altitude of 514.8 km (between 505-533 km), an inclination of 97.44° and a local equator crossing time of 18:00 on the ascending node with a nominal revisit period of 11 days (and 167 orbits in the repeat) [1] [3]. The satellite was launched on June 15, 2007 from Baikonur Cosmodrome, Kazakhstan. The mission had a design life of 5 years with a goal of 6.5 years. As of January 2022, TerraSAR-X is still performing scientific operations in space [1].

The TanDEM-X spacecraft was launched in June 21, 2010 from Baikonur. Given the close formation with TerraSAR-X as required by the SAR mission, it is of no surprise that TanDEM-X has a practically identical orbit. To set up an effective baseline, TanDEM-X is separated in the right ascension of the ascending node with a small offset in eccentricity. A horizontal baseline between the two spacecraft

is maintained between 200 and 3000 m and shifts based on DEM generation requirements at different latitudes.

The relative orbits of the two spacecraft is known as a Helix formation, which allows for relatively small distances between the satellites throughout the absolute orbits while minimizing risk of collision at the poles. This is achieved by combining out-of-plane displacement through different ascending nodes (e.g. $\Delta\Omega = \{300m, 400m, 500m\}$) and radial separation through different eccentricity vectors (e.g $\Delta e = \{300m, 500m\}$). In the Helix formation, there are no crossings between the two orbits, and so arbitrary along-track shifts in the orbits can be performed to finely adjust the baseline [1]. As a result of this formation, maximum radial separation is achieved at the poles and maximum normal separation at the equator.

TanDEM-X was designed with a mission life of 5 years, and as of January 2022 is still providing SAR imagery after 12 years in orbit [1]. Both TanDEM-X and TerraSAR-X are loaded with enough fuel to continue their mission until 2026 [1].

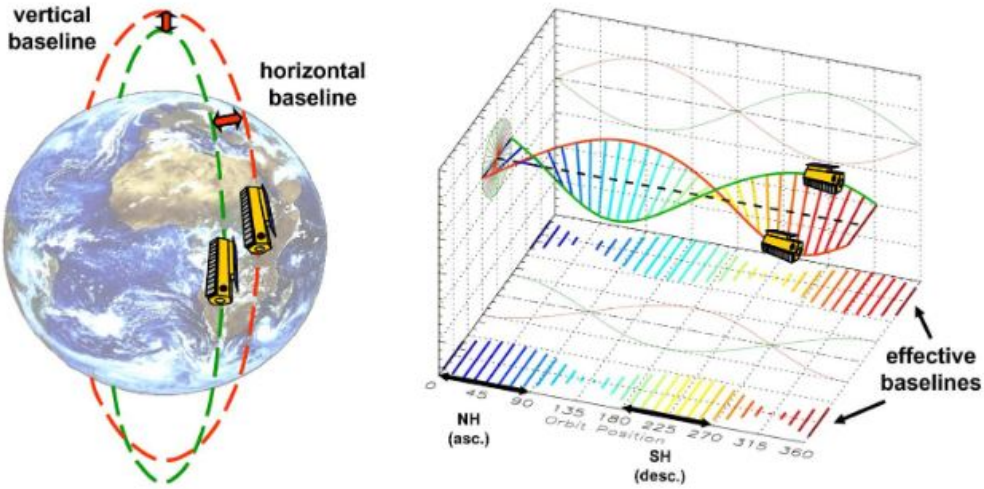

Figure 2: Helix satellite formation of TerraSAR-X and TanDEM-X illustrating relative orbits (left) and cross-track baselines as a function of orbit position (right). [2]

The Science of SAR

The basis of this mission is Synthetic Aperture Radar (SAR), a method of active remote sensing operable during the day, at night, and even through cloud coverage. The technology works by broadcasting a radar signal to the Earth and picking up the reflections. Comparing the reflected signal with the broadcast reveals the nature of the reflector, whether land, water, snow, ice, or otherwise [4]. In the case of TerraSAR-X and TanDEM-X, interferometric SAR can be conducted in four configurations: bistatic, monostatic, alternating bistatic, and simultaneous transmit [2]. A visualization of three of these modes is shown in Figure 3.

- *Bistatic*: This mode is used to generate the DEM. One of the satellites acts as a transmitter over a common radar footprint. Both satellites collect the reflected signals and comparison of the difference generates the DEM [2].
- *Monostatic*: This mode has the satellites acting independently, allowing operators to skip the dif-

ficult synchronization process. With a relatively long baseline (∼10 km), this mode is meant as a backup in case synchronization is not feasible and generates a lower accuracy DEM [2].

- *Alternating bistatic*: This is similar to the bistatic mode, except that the transmitter is switched at every pulse. This mode is used to calibrate the bistatic SAR interferometer [2].
- *Simultaneous transmit*: In this mode both spacecraft transmit at the same time, but the spacecraft maintain a close baseline. This mode allows for further calibration of the SAR instrument [2].

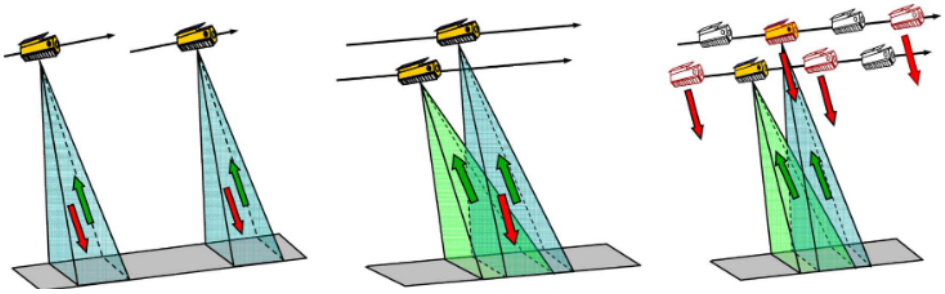

Figure 3: Data acquisition modes: Monostatic (left), bistatic (middle), and alternating bistatic (right). [2]

Key Dynamics, Guidance, Navigation & Control Requirements

For SAR data collection, close-proximity formation-flying while maintaining relative separation is mission-critical. To conduct bistatic interferometry, the satellites must be maintained within a tube 250 m in radius for the duration of the mission [1]. Separation in eccentricity and ascending node is also critical to keep the two satellites in Helix formation and to maximize safety. Radial and normal separation shall not be zero simultaneously to avoid collision.

Furthermore, formation-keeping and localization are crucial for certain SAR operations. Station-keeping thrusters on TanDEM-X regularly fire to counteract drift associated with J2 perturbation. At specific locations of interest, osculating along-track separations must be sufficiently precise to perform along-track interferometry.

Both spacecraft employ GPS, with TerraSAR-X demonstrating an absolute navigational accuracy of 5 cm [1]. The relative baseline between them, which is typically between 500 and 1500 km, has a 1-mm accuracy requirement in order to achieve high-precision DEM [1]. Relative control accuracy requirements are 28 m in cross-track and 200 m in along-track directions, which TanDEM-X has significantly surpassed with nominal accuracies of 5 m in cross-track and 30 m in along-track [1].

2.2 Problem 2: Orbit Simulation, Review of Astrodynamics

Part a

Given the close formation of the two spacecraft, the initial conditions are chosen to be the same orbit for the purposes of this exercise. We pick the initial conditions from TanDEM-X, which was launched on June 21, 2010 into a sun-synchronous orbit with a mean altitude of 514.8 km and inclination of 97.44°. This orbit has a local equator crossing time of 18:00 on the ascending node and was launched on the

summer solstice, corresponding to a right ascension of the ascending node (RAAN) of $\Omega = 270°$. The nominal revisit period is 11 days (and 167 orbits in the repeat). TerraSAR-X flies in a circular orbit and TanDEM-X flies in a slightly eccentric orbit. For this problem, the initial eccentricity is set to $e = 0$. The initial conditions can be described by the following classical Keplerian orbital elements:

$$\begin{array}{ll} a = 6,892.927 \text{ km} & e = 0 \\ i = 97.44° & \Omega = 270° \\ \omega = 0° & f = 0° \end{array}$$

For the following sections, we will use the argument of latitude instead of the true anomaly and argument of periapsis. Since the orbit is circular, the line of apsides is undefined, so the argument of periapsis is undefined (and in practice numerically unstable). The argument of latitude is defined by $u_0 = \omega_0 + f_0 = 0°$. Later on, we will introduce the eccentricity vector / line of apsides to replace the eccentricity as a non-singular orbital element.

Part b

As this is an Earth-centered satellite mission, the inertial reference frame of choice will be Earth Centered Inertial (ECI). The initial Keplerian orbital elements are converted to position and velocity in the ECI frame by first expressing them in the perifocal frame and then performing three coordinate rotations (3-1-3 Euler sequence) about each axis by the right ascension of the ascending node, inclination, and argument of periapsis. In the perifocal frame, position and velocity are given by:

$$^{P}\vec{r} = \frac{a(1-e^2)}{1+e\cos f}\begin{bmatrix}\cos f \\ \sin f \\ 0\end{bmatrix} \tag{1}$$

$$^{P}\vec{v} = \sqrt{\frac{\mu}{a(1-e^2)}}\begin{bmatrix}-\sin f \\ e+\cos f \\ 0\end{bmatrix} \tag{2}$$

The transformation matrix from the perifocal to the ECI frame is given by the following, where R_k represents the direction cosine matrix rotating about the k-axis:

$$R_{PQW}^{ECI} = R_z(-\Omega)R_x(-i)R_z(-\omega) \tag{3}$$

From these equations, the initial position and velocity in the ECI frame is found to be:

$$^{I}\vec{r}_{ECI} = [-892.5 \quad 0 \quad 6834.8]\ km$$
$$^{I}\vec{v}_{ECI} = [0 \quad 7.6045 \quad 0]\ km/s$$

Part c

The orbit tracks shown in Figure 4 depict a constant circular orbit in the unperturbed and perturbed cases. Introducing J2 perturbations causes a nodal precession of the orbit due to the non-spherical mass

distribution of the Earth. The following J2 acceleration was used in ECI [5]:

$$ {}^{I}a_{ECI}^{J2} = \frac{3J_2\mu R_E^2}{2||\vec{r}||^5}\left[(5\frac{r_k^2}{||\vec{r}||^2}-1)(r_i\hat{I}+r_j\hat{J})+(5\frac{r_k^2}{||\vec{r}||^2}-3)r_k\hat{K})\right] $$

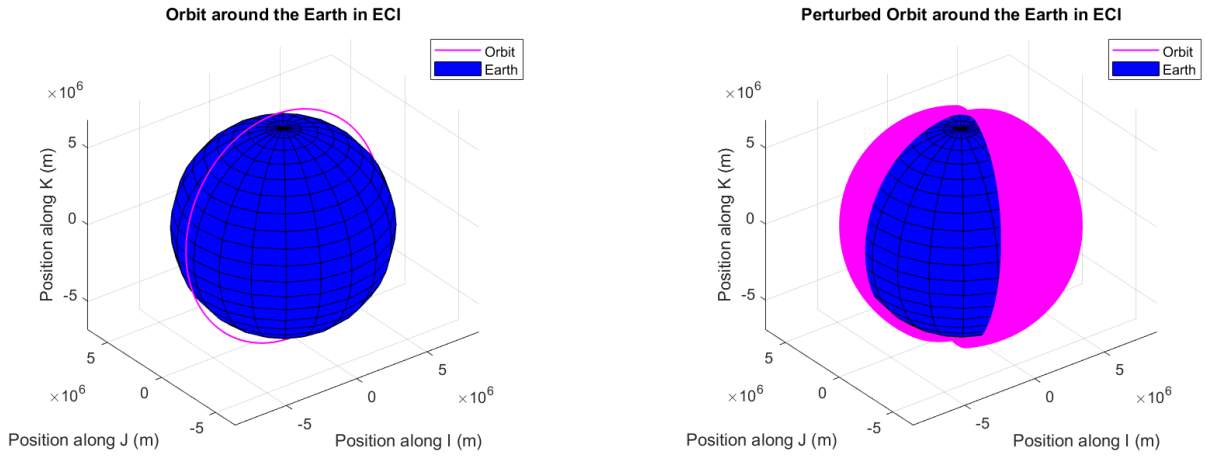

(a) Unperturbed orbit

(b) J2 perturbed orbit

Figure 4: Simulated TanDEM-X orbits on 21 June 2010 (1000 orbits)

Part d

In the restricted two-body problem, the sole parameter varying with time is the mean anomaly M, which is related to the eccentric anomaly E by

$$ M = \sqrt{\frac{\mu}{a^3}}(t-t_0) = E - e\sin E \tag{4} $$

The true anomaly is related to the eccentric anomaly by

$$ \tan\frac{E}{2} = \sqrt{\frac{1-e}{1+e}}\tan\frac{f}{2} \tag{5} $$

Using the same time steps as the numerical integration, Keplerian propagation was determined analytically by incrementing the mean anomaly and transforming mean anomaly into true anomaly, and applying the conic section equations (Eqs. 1 and 2) to resolve the position and velocity in the perifocal frame. Given that we had previously validated code to transform orbital elements to the ECI frame, we used that to get the position and velocity in ECI.

The position vector can be expressed in the Radial, Along-Track, and Cross-Track (RTN) frame by combining the rotation matrix R_{PQW}^{ECI} from Eq. 3 with a subsequent rotation by the true anomaly:

$$ R_{ECI}^{RTN} = R_{PQW}^{ECI}R_z(-f) \tag{6} $$

$$\vec{r}_{RTN} = R_{ECI}^{RTN} \vec{r}_{ECI} \tag{7}$$

Because the RTN frame is a non-inertial reference frame, the Theorem of Coriolis must be applied to express the velocity in RTN in addition to the coordinate transformation:

$$^{RTN}\vec{v}_{RTN} = R_{ECI}^{RTN} \left(^{ECI}\vec{v}_{ECI} + ^{RTN}\vec{\omega}_{ECI}^{ECI} \times \vec{r}_{ECI} \right) \tag{8}$$

where the angular velocity of the ECI frame with respect to the RTN frame, expressed in the ECI frame is simply the rate of change of the true anomaly, $^{RTN}\vec{\omega}_{ECI}^{ECI} = [0, 0, -\dot{f}]^T$.

From Figure 5, we can see that the position error grows to the order of millimeters and the velocity error grows to the order of micrometers per second after ten orbits. These results were obtained using a tolerance of 10^{-12} for the *ode45* solver and a step size of one-hundredth of the orbital period. Increasing either of these two metrics led to an increase in error.

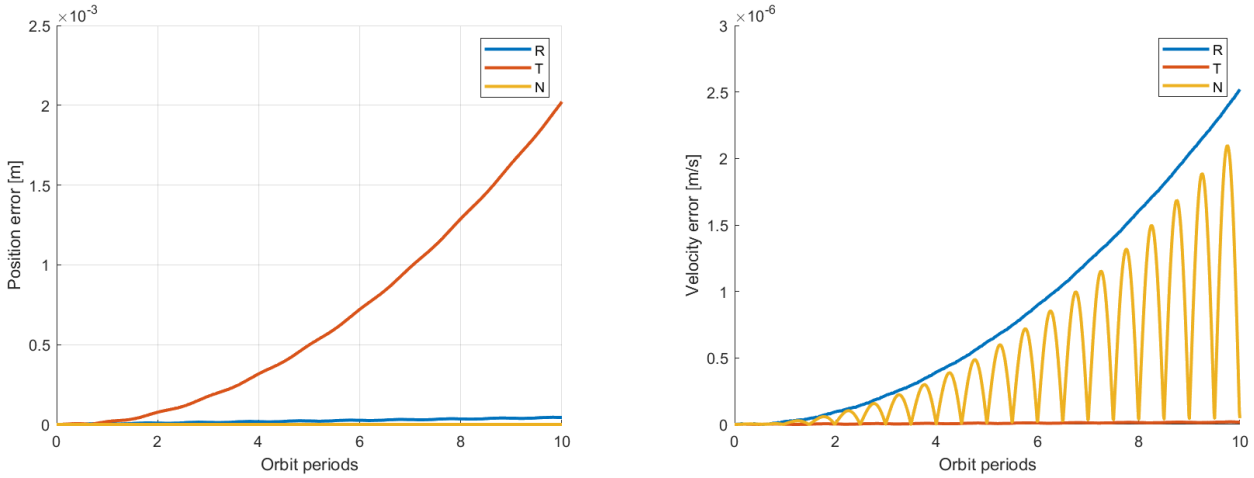

(a) Position error

(b) Velocity error

Figure 5: Position and velocity errors of the numerical integration with respect to the analytical solution in the RTN frame.

Part e

Here we take the steps described in Vallado [6]. The implementation begins by finding three vectors which define typical orbits (specific angular momentum, line of nodes, and line of apsides):

$$^{ECI}\vec{h} = {}^{ECI}\vec{r}x\,{}^{ECI}\vec{v} \tag{9}$$

$$^{ECI}\hat{n} = \hat{K}x\,{}^{ECI}\vec{h} \tag{10}$$

$$^{ECI}\hat{e} = \frac{1}{\mu}\left[\left(||\,{}^{ECI}\vec{v}||^2 - \mu/||\,{}^{ECI}\vec{r}||\right){}^{ECI}\vec{r} - \left({}^{ECI}\vec{r}.\,{}^{ECI}\vec{v}\right){}^{ECI}\vec{v}\right] \tag{11}$$

We can also compute the orbit shape (assuming it is closed, not parabolic):

$$\epsilon = \frac{||^{ECI}\vec{v}||^2}{2} - \frac{\mu}{||^{ECI}\vec{r}||} \tag{12}$$

$$a = -\frac{\mu}{2\epsilon} \tag{13}$$

We then finally find the orientation of the orbit:

$$i = cos^{-1}\left(\frac{h_K}{||^{ECI}\vec{h}||}\right) \tag{14}$$

$$\Omega = cos^{-1}\left(\frac{n_I}{||^{ECI}\hat{n}||}\right) \tag{15}$$

$$u = cos^{-1}\left(\frac{^{ECI}\hat{n} \,.\, ^{ECI}\vec{r}}{||^{ECI}\hat{n}||\,||^{ECI}\vec{r}||}\right) \tag{16}$$

In addition, checks in the code are performed to ensure that these angles are evaluated in the correct quadrants within the range $[0, 2\pi)$.

We see from Figure 6 that for unperturbed orbit propagation, all orbital elements are constant except for the argument of latitude (u). Additionally, the line of apsides defined by the vector e is constant while the specific angular momentum varies as shown in Figure 7. Over a period of 5 orbits, this variance was calculated to be on the order of $1m^2/s$, which is significantly smaller than the magnitude of specific angular momentum ($10^{10}\ m^2/s$). This discrepancy may be attributed to numerical integration errors.

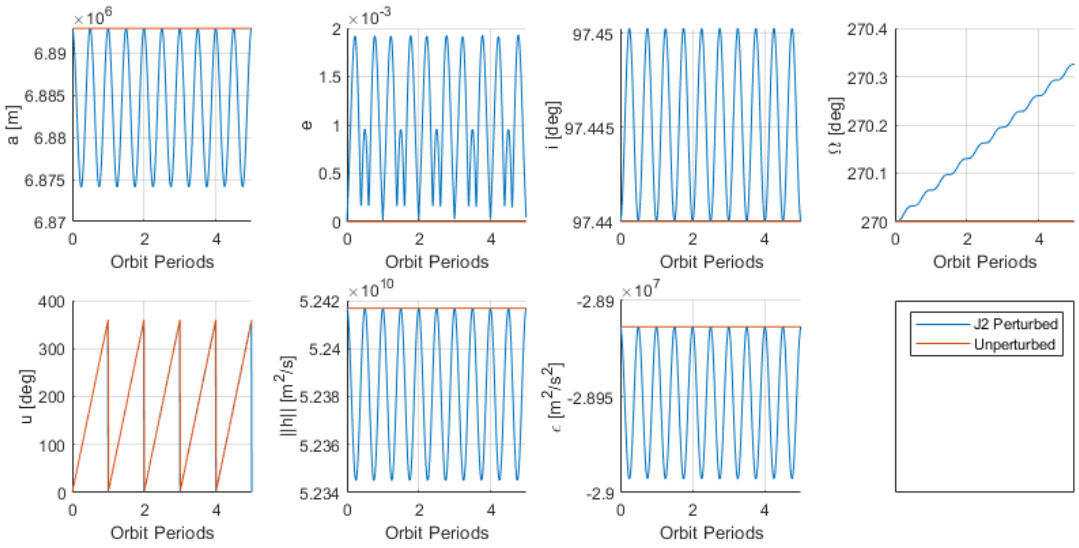

Figure 6: Orbital elements, specific angular momentum, and specific energy over 5 orbits for J2 (blue) and unperturbed (red) propagation.

Including J2 effects (short and long period oscillations), we find that all orbital elements, the specific mechanical energy, the line of apsides and the specific angular momentum exhibit periodicity. The right

ascension of the ascending node Ω is clearly under secular effects as well; as is expected for an inclined orbit. Likewise, we observe that the specific angular momentum demonstrates secular effects along two of the axis, which is also expected given the changes in the right ascension of the ascending node.

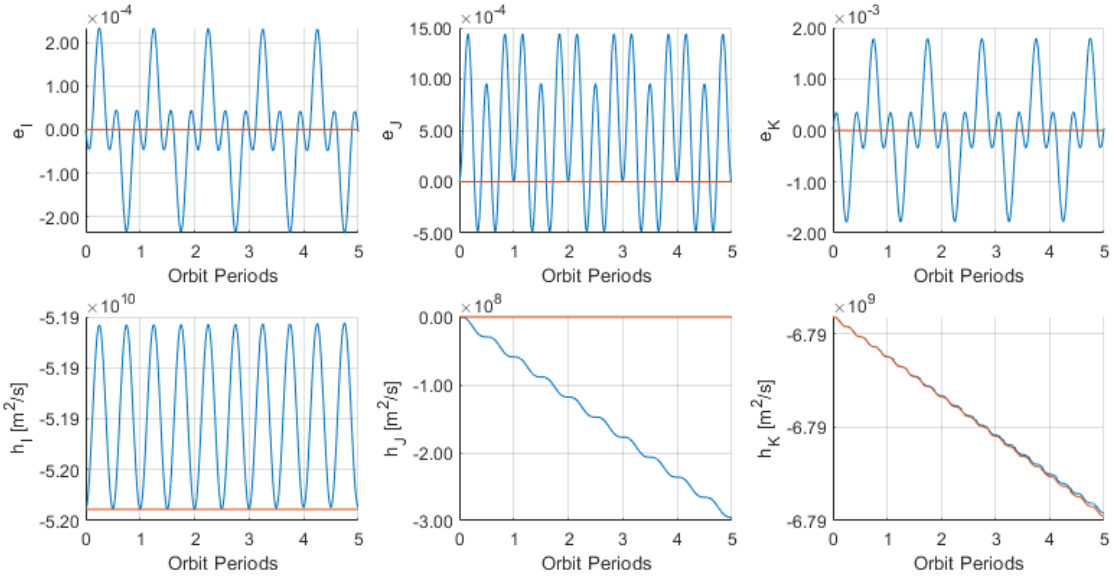

Figure 7: Line of apsides and specific angular momentum over 5 orbits for J2 (blue) and unperturbed (red) propagation.

Part f

The linear differential equations for the mean classical orbital elements reflect zero variation in a, e, and i over time. The following differential equations are used in order to update the new state composed of orbital elements [7]:

$$\frac{d\Omega}{dt} = -\frac{3}{2} n J_2 \left(\frac{R_E}{p}\right)^2 cos(i) \tag{17}$$

$$\frac{du}{dt} = \frac{3}{4} n J_2 \left(\frac{R_E}{a(1-(e_x^2+e_y^2))}\right)^2 \left(\sqrt{1-(e_x^2+e_y^2)}(3cos^2 i - 1) + (5cos^2 i - 1)\right) \tag{18}$$

$$\frac{de_x}{dt} = -\frac{3}{4} n J_2 \left(\frac{R_E}{a(1-(e_x^2+e_y^2))}\right)^2 e_y(5cos^2 i - 1) \tag{19}$$

$$\frac{de_y}{dt} = \frac{3}{4} n J_2 \left(\frac{R_E}{a(1-(e_x^2+e_y^2))}\right)^2 e_x(5cos^2 i - 1) \tag{20}$$

We follow a similar procedure as in the previous section to produce an evolution of the state vector. The orbital elements, specific angular momentum, and specific energy are superimposed with the osculating values in Figure 8.

Under averaging theory, we know the J2 perturbs the right ascension of the ascending node, the argument of periapsis and the mean anomaly. Since we are using the argument of latitude, the effects of the latter two get folded into this one. We see this clearly in Figure 8, where the only secular effects can be seen in

the right ascension of the ascending node. Note that the argument of latitude seems to be unperturbed, however a zoom in in Figure 10 shows that this is precessing. Note that this precession is due to J_2, and that under the averaging theory we ignore motion that is periodic. This is why, unlike in the propagation of the position and velocity state vector, we do not see rapid changes in the argument of latitude as the satellites traverses its orbit.

Additionally, given the equations above, we not would expect a perfectly circular orbit to have any effects on its eccentricity by J_2. In Figure 10, we do see very slight changes, and this is likely a numerical error. When we calculate the initial eccentricity vector we arrive at a practically 0 value, but given the slight numerical error, we are not exactly at 0.

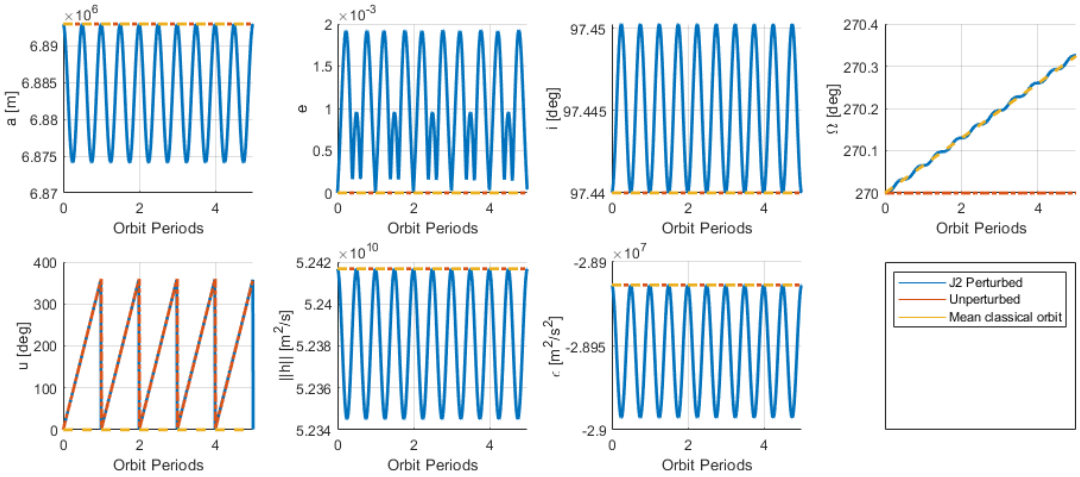

Figure 8: Orbital elements, specific angular momentum and specific energy over 5 orbits for J2 (blue), unperturbed (red), and mean classical (yellow) orbit propagation.

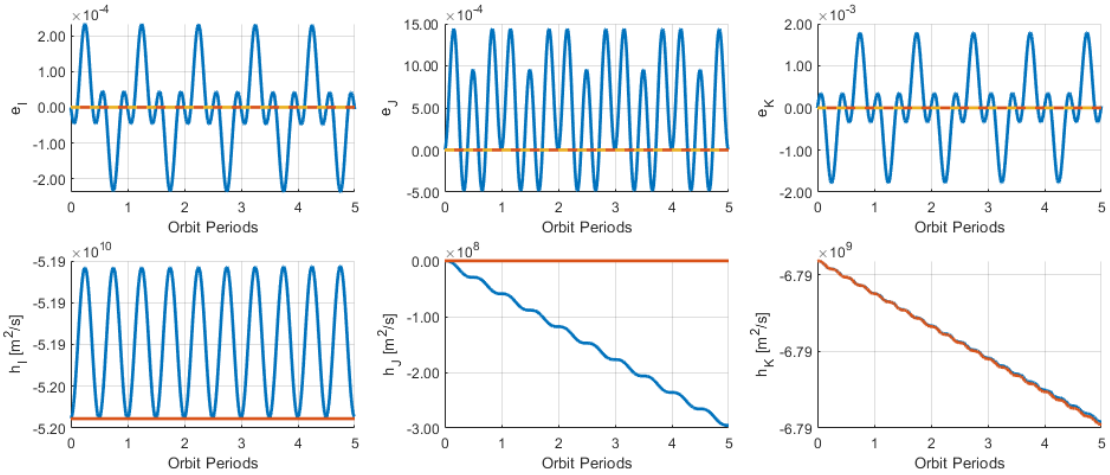

Figure 9: Line of apsides and specific angular momentum over 5 orbits for J2 (blue), unperturbed (red), and mean classical (yellow) orbit propagation.

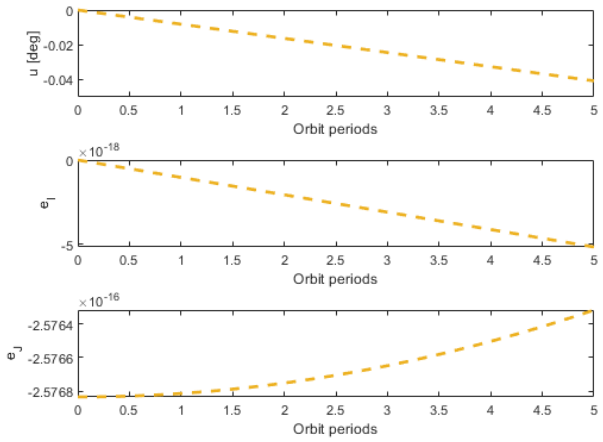

Figure 10: Zoom into seemingly unperturbed parameters of the mean classical orbit propagation.

Part g

Inconsistencies during initialization can be mitigated using Brower theory to transform between mean and osculating values. We see this issue very clearly when comparing the unperturbed elements in the mean classical obit case. Applying Brower theory would allow us to match the behaviour seen in Figure 8 from the mean classical orbit case with the behaviour seen in the J2 perturbed.

3 References

[1] H. J. Kramer. "Tdx (tandem-x)." (Sep. 2016), [Online]. Available: https://www.eoportal.org/satellite-missions/tandem-x.

[2] G. Krieger, A. Moreira, H. Fiedler, *et al.*, "TanDEM-x: A satellite formation for high-resolution SAR interferometry," *IEEE Transactions on Geoscience and Remote Sensing*, vol. 45, no. 11, pp. 3317–3341, Nov. 2007, ISSN: 1558-0644. DOI: 10.1109/TGRS.2007.900693.

[3] H. J. Kramer. "Tsx (terrasar-x)." (Jun. 2012), [Online]. Available: https://www.eoportal.org/satellite-missions/terrasar-x.

[4] A. I. Flores-Anderson, K. E. Herndon, R. B. Thapa, and E. Cherrington, *The Synthetic Aperture Radar (SAR) Handbook: Comprehensive Methodologies for Forest Monitoring and Biomass Estimation*. SERVIR Global Science Coordination Office, Apr. 2019. DOI: 10.25966/nr2c-s697.

[5] R. R. Bate, D. D. Mueller, and J. E. White, *Fundamentals of astrodynamics*, en. New York: Dover Publications, 1971, ISBN: 978-0-486-60061-1.

[6] D. A. Vallado, *Fundamentals of Astrodynamics and Applications*. 1997.

[7] K. T. Alfriend, S. R. Vadali, P. Gurfil, J. P. How, and L. S. Breger, *Spacecraft Formation Flying: Dynamics, Control, and Navigation*. Elsevier Astrodynamics Series, 2010.

4 Appendix 1: Code

All code for this project can be found in the following GitHub repository.